Filtering Non-Significant Quench Points Using Collision Impact in Grassfire Propagation

Dakai Jin[1(✉)], Cheng Chen[1], and Punam K. Saha[1,2]

[1] Department of Electrical and Computer Engineering, University of Iowa, Iowa City, USA
{dakai-jin,heng-chen,punam-saha}@uiowa.edu
[2] Department of Radiology, University of Iowa, Iowa City, USA

Abstract. The skeleton of an object is defined as the set of quench points formed during Blum's grassfire transformation. Due to high sensitivity of quench points with small changes in the object boundary and the membership function (for fuzzy objects), often, a large number of redundant quench points is formed. Many of these quench points are caused by peripheral protrusions and dents and do not associate themselves with core shape features of the object. Here, we present a significance measure of quench points using the collision impact of fire-fronts and explore its role in filtering noisy quench points. The performance of the method is examined on three-dimensional shapes at different levels of noise and fuzziness, and compared with previous methods. The results have demonstrated that collision impact together with appropriate filtering kernels eliminate most of the noisy quench voxels while preserving those associated with core shape features of the object.

1 Introduction

Skeletonization provides a compact yet effective representation of an object while preserving its important topological and geometrical features; see [1,2] for through surveys. Most of the popular skeletonization algorithms [2,3] are based on simulation of Blum's grassfire propagation [4], where quench points are formed when two or more fire fronts collide and the skeleton is constructed from the set of these quench points.

A well-known challenge with skeletonization is that small protrusions and dents on an object boundary create noisy quench points leading to noisy skeletal branches. This challenge is further intensified for fuzzy objects, because local maxima as well as ridges on the membership function create additional noisy quench points. Thus, the skeleton formed by the initial set of quench points consists of a large amount of redundant structures most of which carry little information related to core shape features of the object. Therefore, it is imperative to filter and remove less significant or noisy quench points to produce meaningful skeletons. This paper presents a new filtering algorithm to remove noisy quench points using the collision impact of Blum's grassfire-fronts.

Quench points have been defined and popularly used in skeletonization in the form of centers of maximal balls (CMB) [5]. CMB can be effectively identified in digital objects as the singularity points [5-7] in the distance transform (DT) map [8,9]. Arcel-

V. Murino and E. Puppo (Eds.): ICIAP 2015, Part I, LNCS 9279, pp. 432–443, 2015.
DOI: 10.1007/978-3-319-23231-7_39

li and Sanniti di Baja [5] introduced a criterion to detect the centers of maximal balls (CMBs) from a 3×3 neighborhood in integer-weighted distance transform, and Borgefors [7] extended it to $5 \times 5 \times 5$ neighborhood. Saha and Wehrli [10] generalized the CMB for fuzzy objects, which was further studied by Svensson [11] where the fuzzy distance transform (FDT) [12] is used instead of DT to locate CMBs. Although, a few works [13-16] have been reported in literature to detect noisy or less significant quench points, a comprehensive theoretical formulation for characterization of significance of quench points is yet to emerge. Saha et al. [13] characterized surface- and curve-like shape points and recommended different support kernels to distinguish between noisy and significant quench points. Borgefors and Nyström [14] proposed a CMB reduction algorithm, where a CMB is marked as redundant if the maximal ball centered at it is covered by the union of some other maximal balls. Németh et al. [15] used an iterative boundary smoothing approach to reduce the set of quench points. Recently, Arcelli et al. [16] suggested to a feature-based approach to locate core, relevant and locally convex CMBs as significant ones in skeletonization.

The quench points, i.e., the locations of colliding fire-fronts, have been well-explored in the context of skeletonization in the form of CMBs. However, the measure of collision impact of meeting fire-fronts at quench points has been surprisingly overlooked in both continuous and digital approaches of skeletonization. In this paper, we formulate a new theoretical framework to characterize the significance of a quench point using the collision impact of fire-fronts and explore its role in filtering noisy quench points. The proposed algorithm is uniformly applicable to both binary and fuzzy objects. It uses local characterization of surface and curve quench points to determine the appropriate support kernels and to compute the average collision impact over the support kernel determining the significance of quench points. The new filtering algorithm has been applied to three-dimensional (3-D) binary and fuzzy objects and its performance under different levels of noise and fuzziness is examined. Also, the performance of this is compared with other DT-based methods of distinguishing between noisy and significant quench points [17-20].

2 Theory and Algorithms

In this section, we define the collision impact and describe the intuitive idea behind its relation with skeletal features of an object in the continuous space. A simple expression of collision impact is presented for digital objects. Finally, a filtering algorithm is described using the measure of collision impact to eliminate noisy quench points while preserving those associated with core shape features of the object.

2.1 Collision Impact and Its Relations with Skeletal Features

Distance transform (DT) [8,9,12] defines the time when a fire-front reaches at a given point during Blum's grassfire propagation, and a level set of DT gives a snapshot of the entire fire-front at one time instance. Note that the DT function is not differentiable everywhere (e.g., it is not differentiable at ridge points), but it is

semi-differentiable. Thus, we can compute one-sided directional derivative of DT as follows:

$$\partial_{\mathbf{v}} DT(\mathbf{p}) = \lim_{\Delta \to 0^+} \frac{DT(\mathbf{p} + \Delta \cdot \mathbf{v}) - DT(\mathbf{p})}{\Delta}, \tag{1}$$

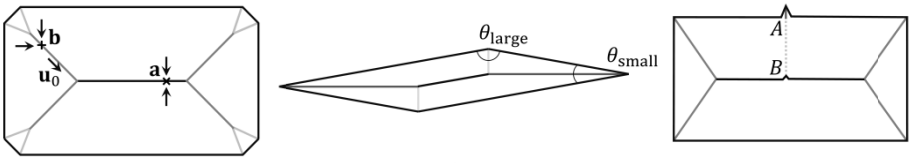

Fig. 1. Collision-impacts at different skeletal points during grassfire propagation on binary shapes. (a) The fire-fronts make head-on collision at the point **a** with the maximum collision-impact of '1'. At the point **b**, the fire-fronts collide obliquely generating a weaker collision-impact. (b) The collision impact along a skeletal branch, originated from a polygonal vertex with a small interior angle, e.g., θ_{small}, is higher than that along a skeletal branch generated from a vertex with a large interior angle, e.g., θ_{large}. (c) The collision-impact along the skeletal branch-segment AB connecting a small protruding structure to the central skeleton, shown by the dotted line, is low.

where $\mathbf{v} \in R^3$ is a direction vector. The uniform speed assumption of Blum's grassfire propagation leads to the following equality for the *speed function* τ at a point $\mathbf{p}$ through which a fire-front passes:

$$\tau(\mathbf{p}) = \max_{\mathbf{v}} \partial_{\mathbf{v}} DT(\mathbf{p}) = 1. \tag{2}$$

The above equality is violated only at *singular* or *quench point*s where multiple fire-fronts collide forming skeletal structures. Although, colliding fire-fronts stop at quench points, their collision strength or impact may vary depending upon the angle between them. The *collision impact* ξ of colliding fire-fronts at a point $\mathbf{p}$ in a binary object is defined as follows:

$$\xi(\mathbf{p}) = 1 - f_+\big(\tau(\mathbf{p})\big) = 1 - f_+\left(\max_{\mathbf{v}} \partial_{\mathbf{v}} DT(\mathbf{p})\right), \tag{3}$$

where the function $f_+(x)$ returns the value of x if $x > 0$ and '0' otherwise.

The intuitive idea behind the formulation of collision impact is explained in Fig. 1 in two-dimension (2-D). Consider the octagonal shape of Fig. 1 (a) and the head-on collision of fire-fronts at the point **a**. At the vicinity of **a**, since, there is no point with its DT value greater than that of **a**, the maximum value of $\partial_{\mathbf{v}} DT(\mathbf{a})$ is zero. Thus, the collision impact $\xi(\mathbf{a})$ takes the highest-possible value of '1'. Now, let us consider the situation at the point **b** where the fire-fronts collide obliquely. Although, the colliding fire-fronts are stopped at **b**, there are increasing DT values at its vicinity. It can be shown that the maximum value of $\partial_{\mathbf{v}} DT(\mathbf{b})$ is achieved along the direction $\mathbf{u}_0$ lying on the tangent space of the skeleton at point **b**. Since, $\partial_{\mathbf{v}} DT(\mathbf{b})$ along $\mathbf{u}_0$ has a finite positive value, the collision impact $\xi(\mathbf{b}) < 1$. As shown in Fig. 1 (b), for a polygonal shape, the collision impact along a skeletal branch originated from a vertex with a small interior angle θ_{small} is large as compared to the collision impact along a skeletal branch originated from a

vertex with a large interior angle θ_{large}. Another important observation on collision-impact is illustrated in Fig. 1 (c). The collision-impact along the skeletal branch-segment AB on the skeletal branch connecting a small protrusion to the central skeletal branch is low. Thus, collision impact assigns a significance measure to individual skeletal or quench points, and an effective algorithms for filtering noisy quench points using collision impact is presented in Section 2.3.

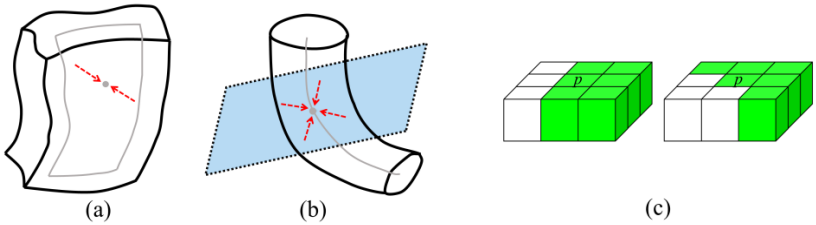

Fig. 2. (a,b) Illustration of surface- (a) and curve-like (b) quench points. (c) Two example support kernels to filter a surface quench voxel. Voxels colored in green are used for average collision impact computation. Four geometrically similar support kernels are constructed from each of these two examples.

2.2 Collision Impact for Digital Objects

In this section, we present a generalized formulation quench points that is applicable to both fuzzy and binary digital objects. Here, a 3-D *cubic grid,* denoted as Z^3, where Z is the set of integers, is used as the image space. Each grid element $p = (p_x, p_y, p_z) \in Z^3$ is referred to as a *voxel*. Traditional definitions of *α-adjacent* or *α-neighborhood* [1] between two voxels $p, q \in Z^3$, where $\alpha \in \{6,18,26\}$, are followed in this paper. $N_{26}(p)$ is used to denote the set of 26-neighbors of a voxel p including p itself while $N_{26}^*(p)$ is used for the set of all voxels of $N_{26}(p)$ excluding the central voxel p. Moreover, the traditional definitions of *α-path*, *α-connectedness*, *and α-components* [1] are followed in this paper.

A fuzzy digital object $\mathcal{O} = (O, f_{\mathcal{O}})$, is a fuzzy set of Z^3, where $f_{\mathcal{O}}: Z^3 \rightarrow [0,1]$ is the *membership function* and $O = \{p \in Z^3 | f_{\mathcal{O}}(p) > 0\}$ is its support. Here, 26-adjacency is used for object voxels in O, while 6-adjacency is used for background voxels, i.e., voxels in $\bar{O} = Z^3 - O$. A binary object $\mathcal{B}$ is defined similarly except that the membership function $f_{\mathcal{B}}: Z^3 \rightarrow \{0,1\}$ takes the value of '1' for object voxels and '0' for background voxels. A voxel p is a CMB in a fuzzy object $\mathcal{O}$, if the following inequality holds for every $q \in N_{26}^*(p)$ [10],

$$FDT(q) - FDT(p) < \frac{1}{2}\left(f_{\mathcal{O}}(p) + f_{\mathcal{O}}(q)\right)|p - q|. \tag{4}$$

Following the formulation of the collision impact in the continuous space in Eq. 3, the collision impact at any voxel p in fuzzy object $\mathcal{O}$, denoted by $\xi_D(p)$, is defined as follows:

$$\xi_D(p) = 1 - \max_{q \in N_{26}^*(p)} \frac{f_+\left(FDT(q) - FDT(p)\right)}{\frac{1}{2}\left(f_{\mathcal{O}}(p) + f_{\mathcal{O}}(q)\right)|p - q|}. \tag{5}$$

2.3 The Filtering Algorithm for Noisy Quench Voxels

The new algorithm for filtering noisy quench points works in the following steps – (1) detect surface- and curve-type quench voxels, (2) determine support kernels for each quench voxel depending on its type, and (3) analyze the collision impact over the support kernels and determine the significance of the quench voxel, and (4) remove quench voxels with their significance measure falling below a predefined threshold. These steps are described in the following.

Both surface- and curve-quench points may form in 3-D (Fig. 2). A *surface quench point* is formed when two opposite fire fronts meet, while a *curve quench point* is formed when co-planar fire fronts meet from all directions. In the digital space, a *surface-quench voxel* is formed by opposite fire fronts along x-, y- or z-direction and a *curve-quench voxel* is formed by fire fronts meeting from all eight directions on xy-, yz-, or zx-planes. See [13,21] for formal definitions of surface and curve quench voxels.

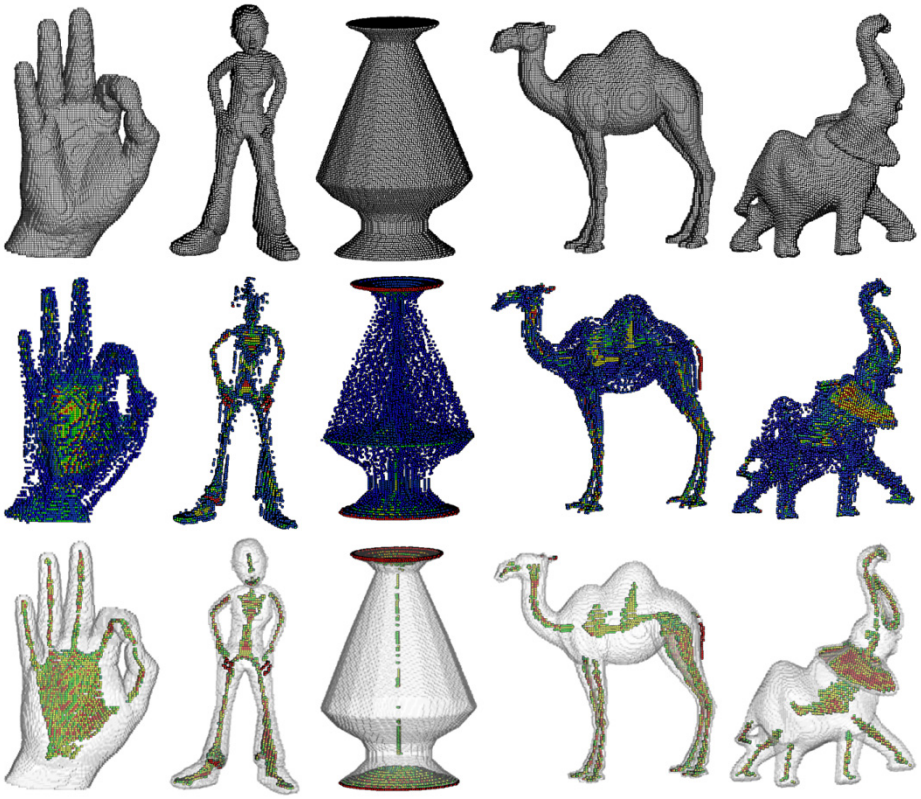

Fig. 3. Results of the collision impact and filtering method on 3-D objects. The top row shows the original binary objects, while the second and third rows show the initial and filtered quench voxels with color-coded collision impacts. The fourth and fifth rows present the initial and filtered quench voxels in fuzzy objects generated by down-sampling.

Fig. 3. (*Continued*)

To determine the significance of a surface-type quench voxel, a support kernel on a 3×3 digital surface orthogonal to the surface-normal direction is constructed and the significance is determined as the average collision impact over the support kernel (Fig. 2 (c)). For a curve-type quench voxel with the horizontal cutting plane, its significance is defined as the maximum collision impact over the support kernels of 3×3 digital surfaces on either side of the cutting plane. These processes are defined in the following. Let $p = (p_x, p_y, p_z)$ be an x-surface quench voxel. To compute the support for p, first, a projection of three voxels $\{q_{i,j}^+ = (p_x - 1, p_y + i, p_z + j), q_{i,j} = (p_x, p_y + i, p_z + j), q_{i,j}^- = (p_x + 1, p_y + i, p_z + j)\}$, for some $i, j \in \{-1,0,1\}$, is computed to generate a 3×3 field of significance map $M_p^{\mathrm{x}}(i,j)$ as follows:

$$M_p^{\mathrm{x}}(i,j) = \max\{\xi_D(q_{i,j}^+), \xi_D(q_{i,j}), \xi_D(q_{i,j}^-)\}.$$

The average significance value m_i^{x} over each of eight different support nels$D_i \mid i = 1, \cdots, 8$ (see Fig. 2 (c)) is computed. An x-surface-quench voxel p is referred to as *x-significant surface-quench* voxel, if any of the average values $m_i^{\mathrm{x}} \mid i = 1, \cdots, 8$ is greater than a preset threshold. A voxel p is referred to as a *significant surface-quench* voxel if it is an x-, y-, or z-significant surface-quench voxel. An xy-curve-quench voxel $p = (p_x, p_y, p_z)$ is an xy-significant curve-quench voxel if the largest collision impact value in either of the two 3×3 planar cliques $C_{\mathrm{z}}^+ = \{(p_x + i, p_y + j, p_z + 1) \mid i, j \in \{-1,0,1\}\}$ and $C_{\mathrm{z}}^- = \{(p_x + i, p_y + j, p_z - 1) \mid i, j \in \{-1,0,1\}\}$ is greater than a preset threshold. An xy-, yz-, or zx-significant curve-quench voxel is referred to as a *significant curve-quench* voxel. A significant surface- or curve-quench voxel is referred to as a *significant quench voxel*. In this paper, a constant threshold of 0.5 and 0.75 are used for the significance of surface- and curve-quench voxels, respectively.

3 Experiments and Results

Results of the filtering algorithm on a 3-D shape of dinosaur are presented in Fig. 4. Online shapes were constructed at 512×512×512 arrays, which were down-sampled by a window of 4×4×4 voxels to generate test phantoms. The binary objects (top row) were generated by thresholding test phantoms at 0.5, while the test phantoms were directly used as fuzzy objects (not shown in the figure). The initial set of quench voxels for binary objects with color-coded collision impact values (blue = 0.0, cyan = 0.25, green = 0.5, yellow = 0.75, and red = 1.0) are illustrated on the second row of the figure, while the filtered quench voxels are shown on the third row. It is observed that that the filtering algorithm has removed visually evident noisy quench voxels while preserving the ones capturing the core skeletal shapes of individual objects. Initial quench voxels and the filtered ones for fuzzy objects are presented on the last two rows. It is observed that the initial sets of quench voxels for fuzzy objects are larger than that of binary objects. Despite the additional initial quench voxels for fuzzy objects, the filtering algorithm produced satisfactory results. The visual agreement among the filtered significant quench voxels for binary and fuzzy objects is highly encouraging that suggests that the algorithm is robust in the presence of partial voluming in fuzzy objects.

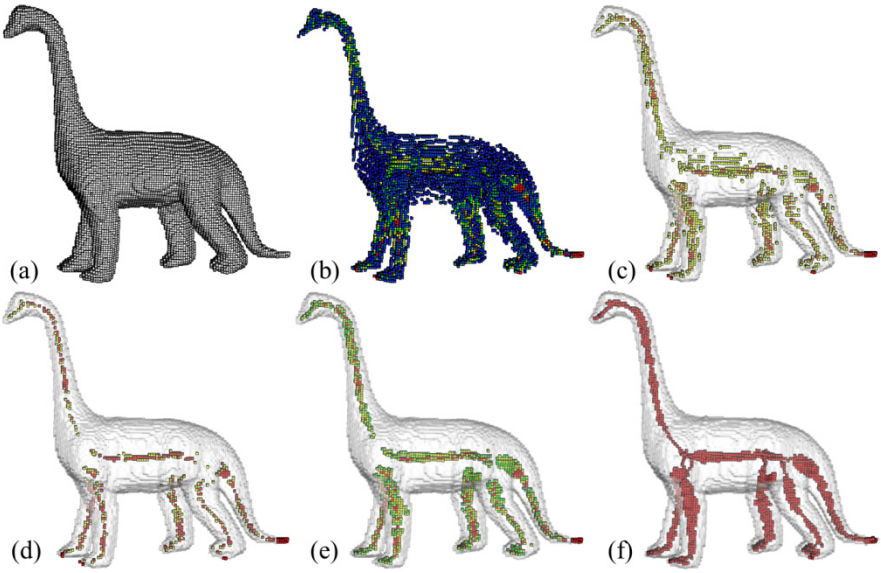

Fig. 4. An example of the collision impact and the filtering results on a 3-D shape. (a) The original binary object; (b) initial quench voxels with color-coded collision impact; (c,d) quench voxels after thresholding at the collision impact using of 0.6 (c) and 0.7 (d); (e) significant quench voxels after filtering; (f) final skeleton.

Results of the filtering algorithm on a 3-D shape of dinosaur are presented in Fig. 3 and its performance is compared with simple thresholding on collision impact. Although, a thresholding on collision impact partially works in the sense that most

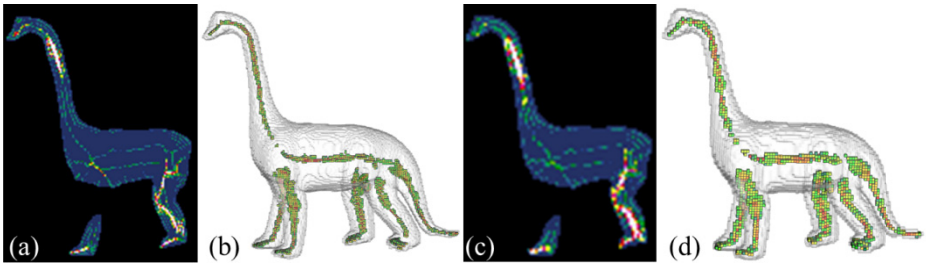

Fig. 5. Results of the collision impact and the filtering algorithm on dinosaur shape at two down-samplings of 3×3×3 and 5×5×5 voxels. (a, c) 2-D slice showing the distribution of quench voxels along with their collision impacts values. (b, d) 3-D results of the filtered quench voxels using the proposed method.

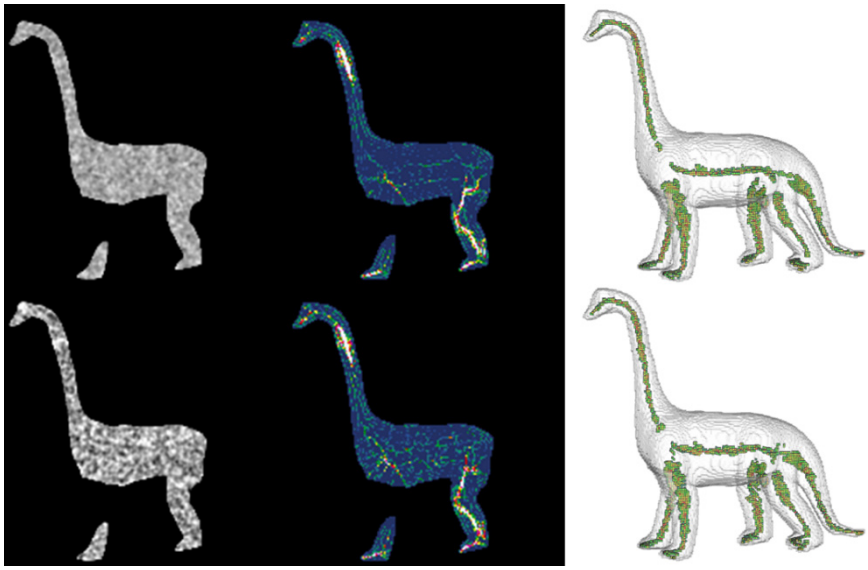

Fig. 6. Results of the collision impact and filtering algorithm on dinosaur shape under two levels of membership noises, at SNR24 (top row) and SNR6 (bottom row), respectively. Left column shows a 2-D slices from noisy object. Middle column shows the distribution of quench voxels along with their collision impact values. Right column displays the result of the filtered quench voxels by the proposed method in 3-D.

peripheral and noisy quench voxels are removed and most of the core quench voxels are preserved, the performance is still suboptimal. At the threshold of 0.6, several isolated noisy quench voxels have survived, while an over-deletion of quench voxels has occurred at the threshold of 0.7. On the other hand, the filtering algorithm has removed all visually evident noisy quench voxels while avoiding over-deletion. Finally, note that the quench voxels get connected in the final skeleton due to the topology preservation criterion [22,23] during a thinning process. The performance of the filtering algorithm under different levels of fuzziness and membership noise are presented

in Fig. 5 and Fig. 6. Initial quench voxels on an image slice for two fuzzy objects at 3×3×3 and 5×5×5 down-sampling are presented in Fig. 5a and c. The filtered quench voxels for the two fuzzy objects are shown in Fig. 5b and d. No visually apparent difference in the initial sets of quench voxels is observed. The filtered set of quench voxels at two different levels of fuzziness is visually satisfactory. To study the behavior of the quench voxel generation and the filtering algorithm under membership noise, two fuzzy objects were generated at 3×3×3 down-sampling and then adding white Gaussian noise at signal to noise ratio (SNR) of 24 and 6 (top and bottom rows of Fig. 6, respectively). Visual difference in initial sets of quench voxels are observed at two different levels of noise. Despite the presence of high membership noise, the filtering method successfully eliminated noisy quench voxels while preserving the significant ones.

The performance of the algorithm under different levels of boundary noise is presented in Fig. 7. Three images were generated by randomly adding noisy balls of radius one, two, and three voxels. The sets of quench voxels after thresholding at collision impact values of 0.6 and 0.7 are shown on the second and the third rows, respectively. The sets of filtered quench voxels are presented on the last row. Due to boundary noise, several noisy quench voxels survived even after thresholding at a high value of 0.7 for collision impact. In contrast, the filtering algorithm has successfully removed noisy quench voxels, while preserving the core ones. Finally, as observed from Fig. 5 to Fig. 7, the filtered set of quench is visually similar and stable at wide ranges of boundary noise, down-sampling as well as membership noise. It further enforces the validity of the principle of our noisy quench voxel filtering algorithm.

The performance of the method at different boundary noise levels is compared with the performance of three existing DT-based methods [17-20] on distinguishing between noisy and significant quench voxels. Gagvani and Silver [17] used the difference of the DT value of a quench voxel from the average DT value of its neighbors as its significance. Siddiqi et al.[20] computed the average outward flux of the DT gradient field as a measure of significance of a quench voxel. Shah [18,19] used the largest angle between incoming fire-fronts as the significance of quench voxels. Results of applications of the three methods are presented in Fig. 8. Gagvani and Silver's method failed to remove several visually noisy quench voxels while discontinuities on meaningful skeletal segments become apparent. Shah's method fail to locate quench voxels in the neck, tail, or the legs of the dinosaur. The performance of Siddiqi et al. is more comparable to ours at low noise. However, the performance deteriorated at higher levels of noise where it failed to clean a significant number of noisy voxels.

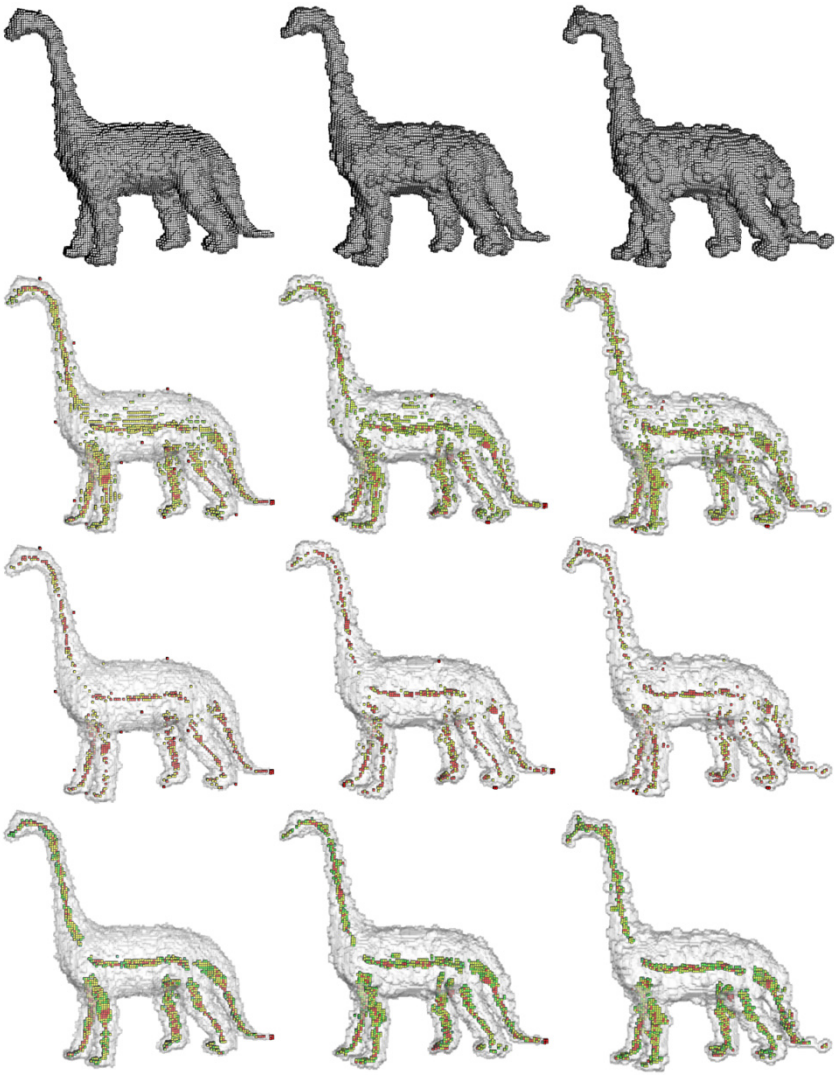

Fig. 7. Results of the collision impact and the filtering algorithm on a binary dinosaur shape under three levels of boundary noises. The top row shows the 3-D volume of binary objects. The second and third row show the quench voxels thresholded at collision impact values of 0.6 and 0.7, respectively. The bottom row displays the filtered quench voxels by the proposed method.

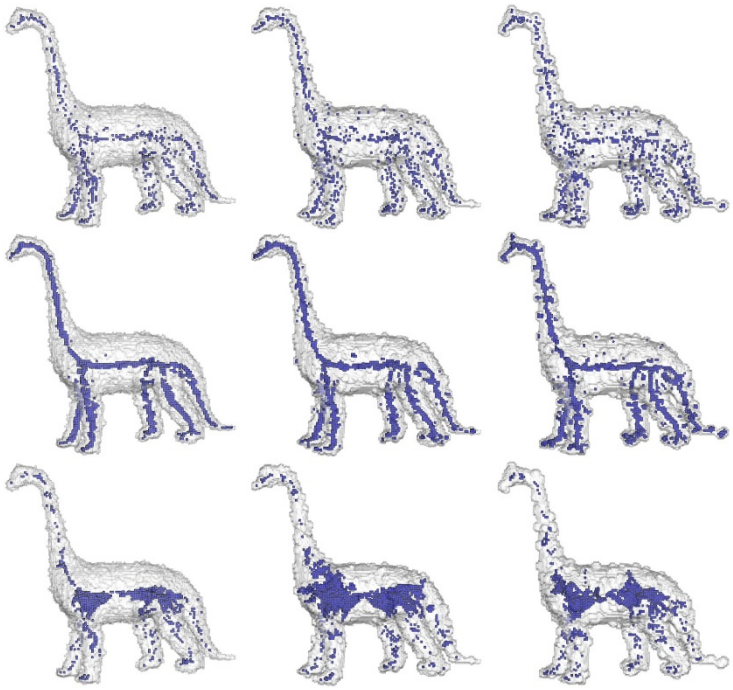

Fig. 8. Results of applications of the DT-based noisy quench voxel filtering methods by Gagvani and Silver [17] (top row), Siddiqi et al. [20] (middle row), and Shah [18,19] (bottom row) on the binary dinosaur shape under three different levels of boundary noise used in Fig. 7.

4 Conclusions

This paper has presented a new theoretical framework to characterize the significance of a quench point using the collision impact of Blum's grassfire-fronts. Its role in filtering noisy quench points, prevalent in the skeletonization of real objects, has been explored. Experimental results have demonstrated the effectiveness of method in removing noisy quench voxels while preserving the significant ones capturing core shape features in both binary and fuzzy objects. Initial results has suggested that the method is stable over wide ranges of boundary noise, down-sampling, and membership noise and generates visually satisfactory results despite significant image artifacts. Our method offers a unified solution for both binary and fuzzy objects, while existing methods are applicable to binary objects, only. Also, the initial results suggests that the current method may perform better as compared to existing ones, especially, at higher levels of noise. Currently, we are conducting quantitative analysis of its performance and exploring its role in improving the results of skeletonization.

Acknowledgements. This work was supported by the NIH grant R01-AR054439.

References

1. Saha, P.K., Strand, R., Borgefors, G.: Digital topology and geometry in medical imaging: a survey. IEEE Trans. Med. Imag. (in press)
2. Saha, P.K., Borgefors, G., Sanniti di Baja, G.: A survey on skeletonization algorithms and their applications. Pat. Reog. Lett. (in press)
3. Siddiqi, K., Pizer, S.M.: Medial representations: mathematics, algorithms and applications. Springer (2008)
4. Blum, H.: A transformation for extracting new descriptors of shape. Model. Percep. Speech Vis. Form **19**, 362–380 (1967)
5. Arcelli, C., Sanniti di Baja, G.: Finding Local Maxima in a Pseudo-Euclidean Distance Transform. Comp. Vis. Grap. Im. Proc. **43**, 361–367 (1988)
6. Borgefors, G., Ragnemalm, I., di Baja, G.S.: The Euclidean distance transform: finding the local maxima and reconstructing the shape. In: Proc 7th Scand. Conf. Imag. Anal., vol. 2, 974–981 (1991)
7. Borgefors, G.: Centres of maximal discs in the 5-7-11 distance transform. In: 8th Scandinavian Conference on Image Analysis, Tromsø, Norway, pp. 105–111 (1993)
8. Borgefors, G.: Distance transform in arbitrary dimensions. Comp. Vis. Grap. Im. Proc. **27**, 321–345 (1984)
9. Borgefors, G.: Distance transformations in digital images. Comp. Vis. Grap. Im. Proc. **34**, 344–371 (1986)
10. Saha, P.K., Wehrli, F.W.: Fuzzy distance transform in general digital grids and its applications. In: 7th Joint Conference on Information Sciences, pp. 201–213. Research Triangular Park, NC (2003)
11. Svensson, S.: Aspects on the reverse fuzzy distance transform. Patt. Recog. Lett. **29**, 888–896 (2008)
12. Saha, P.K., Wehrli, F.W., Gomberg, B.R.: Fuzzy distance transform: theory, algorithms, and applications. Comp. Vis. Imag. Und. **86**, 171–190 (2002)
13. Saha, P.K., Chaudhuri, B.B., Majumder, D.D.: A new shape preserving parallel thinning algorithm for 3D digital images. Pat. Recog. **30**, 1939–1955 (1997)
14. Borgefors, G., Nyström, I.: Efficient shape representation by minimizing the set of centres of maximal discs/spheres. Pat. Recog. Lett. **18**, 465–471 (1997)
15. Németh, G., Kardos, P., Palágyi, K.: Thinning combined with iteration-by-iteration smoothing for 3D binary images. Graph. Mod. **73**, 335–345 (2011)
16. Arcelli, C., Sanniti di Baja, G., Serino, L.: Distance-driven skeletonization in voxel images. IEEE Trans. Patt. Anal. Mach. Intell. **33**, 709–720 (2011)
17. Gagvani, N., Silver, D.: Parameter-controlled volume thinning. Graph. Mod. Imag. Proce. **61**, 149–164 (1999)
18. Shah, J.: Gray skeletons and segmentation of shapes. Comp. Vis. Imag. Und. **99**, 96–109 (2005)
19. Shah, J.: Skeletons of 3D shapes. In: Kimmel, R., Sochen, N.A., Weickert, J. (eds.) Scale-Space 2005. LNCS, vol. 3459, pp. 339–350. Springer, Heidelberg (2005)
20. Siddiqi, K., Bouix, S., Tannenbaum, A., Zucker, S.W.: Hamilton-Jacobi Skeletons. International Journal of Computer Vision **48**, 215–231 (2002)
21. Jin, D., Saha, P.K.: A new fuzzy skeletonization algorithm and its applications to medical imaging. In: Petrosino, A. (ed.) ICIAP 2013, Part I. LNCS, vol. 8156, pp. 662–671. Springer, Heidelberg (2013)
22. Saha, P.K., Chaudhuri, B.B.: Detection of 3-D simple points for topology preserving transformations with application to thinning. IEEE Trans. Patt. Anal. Mach. Intell. **16**, 1028–1032 (1994)
23. Saha, P.K., Chaudhuri, B.B.: 3D digital topology under binary transformation with applications. Comp. Vis. Image. Und. **63**, 418–429 (1996)